Appendix :

## 1. Material and methods: Data processing

### 1.1. Field measurements

We conducted the field surveys in one of the main branches of the Mekong estuary during both the high flow and low flow hydrological seasons.

For each vertical profile, we obtained SSC (in g/L), Particle Size Distribution (PSD in µm) and calibration of turbidity probes by water sampling. 1 litre of water was collected at the surface, at the bottom of the river, and at 5 metres below the water surface (when water depth was exceeding 7m). The sampling depth was controlled with a pressure sensor, before pumping water with a peristaltic pump (Teledyne ISCO Portable Water Sampler). In total, 243 samples were collected at various depths and times (see Table A1).

| Location | Type of parameter | Instrument | Start date | End date | Number |
|---|---|---|---|---|---|
| T1, T2, T3 | Flow, velocity | ADCP | 10/12/2015<br>10/03/2016 | 12/12/2015<br>13/03/2016 | 169<br>181 |
| T1, T3 | Temp, depth, salinitiy, turbidity | Hydrolab probe | 10/12/2015<br>10/03/2016 | 11/12/2015<br>13/03/2016 | 37<br>72 |
| T1, T3 | Water sample | Bottles | 10/12/2015<br>10/03/2016 | 11/12/2015<br>13/03/2016 | 74<br>169 |

**Table. A1.** Numbers of water samples taken and list of the physical quantities measured during field campaigns.

### 1.2. Measure of Suspended Sediment Concentration (SSC)

We measured suspended sediment concentration (SSC) on all samples collected in the field and in the laboratory. Samples were filtered by using pre-weighed microfiber filter papers. After filtration, the filters were dried for 2 h at 105 °C and weighed with a high precision balance (precision ±0.1 mg). In the case of very high SSC exceeding 5.0 g/L, a known volume of sample was dried during 24 h at 60 °C and the residue was weighed. The SSC-turbidity calibration curve was robust for both field and laboratory measurements, with a coefficient of determination R2 higher than 0.98 (see, Fig. A2).

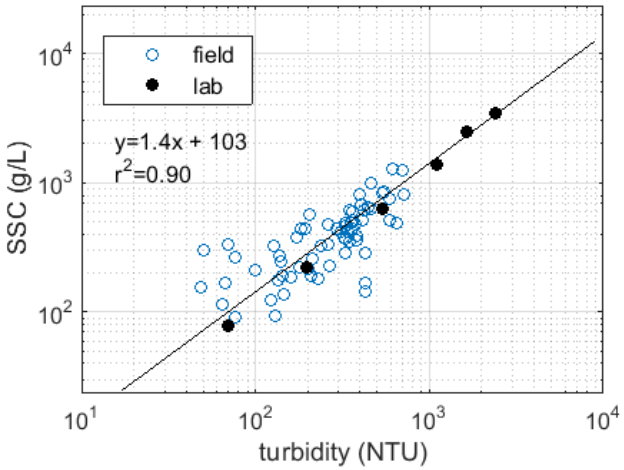


Fig. A1. Variation of suspended sediment concentration (SSC) with turbidity for field and laboratory measurements.

### 1.3. Measure of particle size distribution (PSD) and floc diameter $D_f$

Particle size distribution (PSD) in the water column is a key parameter to understand the sediment dynamics. We use the terminology as in Lee et al. (2014). It discriminates individual primary particles of about one micron from flocculi of a few microns, micro-flocs of some tens of microns, and macro-flocs of hundreds of microns. We determined the particle size distribution with a LISST Portable XR instrument from Sequoia ©. The principle of operation is based on laser diffraction. This instrument provides a semi-log distribution of the volumetric concentration of particles over a 44 bands spectrum from 0.4 to 460 µm. Each spectrum was then sub-divided into independent semi-log sub-populations using a method developed by Launay (2014). This post-processing technique revealed to be useful to prevent misinterpretation resulting from bubbles and or other artefacts that can be observed on the raw spectrum. Each validated sub-population was characterized by its mean particle size Df, its standard deviation σDf and its relative volumetric concentration. For each sample presented in this study a first measurement was done after sampling and a second measurement was performed after two minutes of sonication. The comparison of the PSDs obtained before and after sonication enables a differentiation into the proportion of sand and of flocs, i.e. large particles built by smaller cohesive particles (silt or clay), which are destroyed by the sonication.

### 1.4. Measure of the particles settling velocity and of the flocculation by differential settling

The SCAF settling tube (System for the Characterization of Agregates and Flocs) is an optical settling column, equipped with a vertical array of sixteen optical sensors (Gratiot et al., 2015). In the SCAF instrument, some detailed characteristics of floc settling velocities are deduced from the decrease of

turbidity over time (Mercier et al., 2016; Wendling et al., 2015). Measurements taken in the upper part of the SCAF settling tube during the first minutes provided an estimation of flocs settling velocity under quiescent conditions ws,q (step 2a), while measures realized near the bottom of the settling tube after several tens of minutes provided an estimation of flocs settling velocity by differential settling under settling dominated conditions ws,≠ (step 2b).

### 1.5. Measure of the turbulent dissipation parameter G

Part of the laboratory experiments presented bellow were conducted in a JAR tank, under controlled turbulent conditions.

An Acoustic Doppler Velocity Profiler (Nortek Vectrino2) was immersed in the fluid in order to measure the 3D turbulent field of velocity and deduce the mean turbulent energy dissipation rate G. The mean turbulent energy dissipation rate G is calculated as:

$$G = \sqrt{\frac{\varepsilon}{\nu}} = \sqrt{\frac{u^3}{\nu l}} \qquad \text{(Eq. A1)}$$

with $\nu = 10^{-6}$ ($m^2\ s^{-1}$) the kinematic viscosity of water

$u$ (m s-1) : the time averaged turbulent velocity fluctuations,

$l$ (m) : the integral length scale estimated from the cross-covariance of the velocities along the profile.

It is important to note that using the whole velocity profile enables the estimation of the integral length scale $l$, while $u$ is extracted at the one-third of the profile where the measurement is known to be the most reliable (see e.g. Koca et al., 2017). The dissipation rate of turbulent kinetic energy $\varepsilon$ is also estimated from the inertial subrange of the power spectrum, leading to similar results.

As shown in Fig. A3, measurements fitted well with the theoretical law previously established by Logan (1999) and reported by Keyvani and Strom (2014):

$$G = \left(\frac{0.87\, b_{dp} A_p S^3 R_p^3}{\nu V_T}\right)^{1/2} \qquad \text{(Eq. A2)}$$

with

$b_{dp} = 0.4$ ,

$A_p = 7.6 \times 0.7 \times 10^{-4}$ m2 : the cross sectional area of the paddle,

$S$ (round per minutes) : the impeller rotation speed

$R_p = 0.5 \times 7.6 \times 10^{-2}$ m: the impeller radius

$V_T = 11.5 \times 11.5 \times 15 \times 10^{-6}$ m3: the volume of fluid in the tank

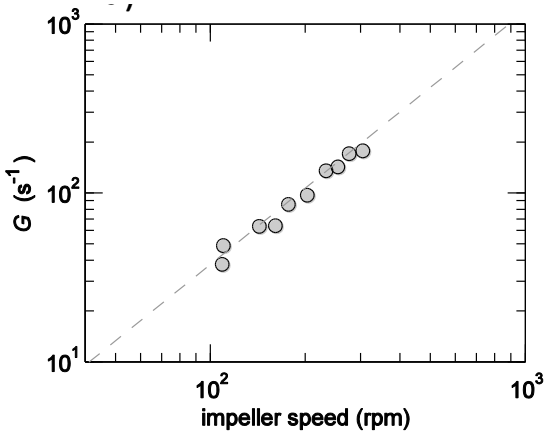


Fig. A2. Variation of the mean turbulent energy dissipation rate G (in s-1) with impeller speed (rpm) under clear water conditions.

1.6. Design of the laboratory experiment

On March 13th 2016, we sampled 5 litres of fluid mud near the bottom of transect T3 in order to carry out further analysis in the laboratory. The salinity of the sample used for lab experiments was 17. Laboratory investigations were undertaken in the Ho Chi Minh University of Technology, in the Asiatic Center for Water Research (CARE). Before performing the experiments, the fluid mud was stored in a dark and hermetic tank at 6°C during 24 hours.

The design of the experimental set-up was based on the conceptual diagram of Dyer (1989) reproduced in Figure A3. This diagram establishes a relationship between the mean turbulent energy dissipation rate G (in $s^{-1}$), the suspended sediment concentration (SSC in g/L) and the mean floc diameter $D_f$ (in µm). As depicted in this figure, the mean floc size of a population (blue curve surface in Fig. A1) results from a dynamic equilibrium between floc breakage by collision or internal shearing (Gratiot and Manning, 2004; Kranenburg, 1994) and flocculation. In Dyer's diagram (1989), $D_f$ can vary over more than one order of magnitude for different concentrations and levels of turbulence. For high turbulence levels above 20-50 $s^{-1}$, Dyer's diagram predicts a predominance of floc breakage, so that the size of aggregated particles does not exceed a few microns. Optimal conditions of flocculation are expected to occur under quiescent conditions or gentle turbulence (a few $s^{-1}$) and for suspended sediment concentration as high as SSC=10 g/L.

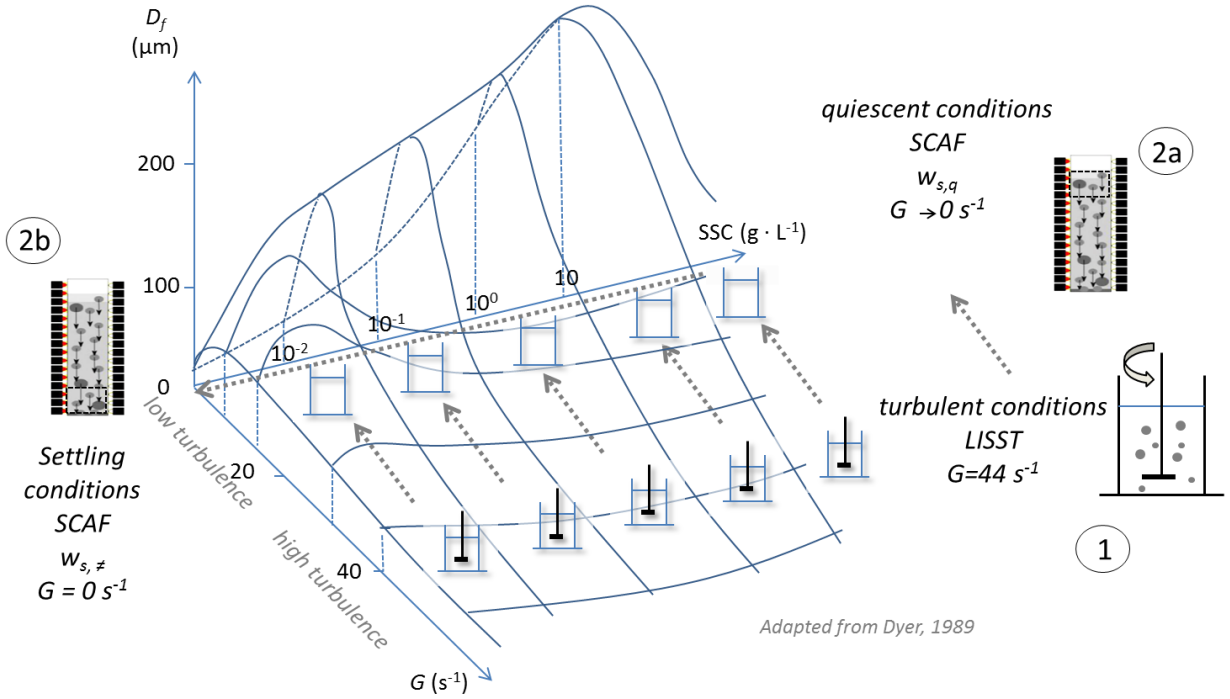


Fig. A3. Experimental procedures superimposed on the conceptual diagram of Dyer (1989). Experiments are first conducted in a jar tank under turbulent dominated conditions (step 1) and secondly in SCAF (System for the Characterisation of Aggregates and Flocs; Gratiot et al., 2015) system under settling dominated conditions (step 2a and 2b).

The laboratory investigations consisted of **two steps** aiming at characterising turbulence, quiescent and settling dominated conditions. The strategy was to cover a wide range of situations in Dyer's diagram with a reasonable number of runs. In total, 21 experiment runs were performed for SSC values covering a wide range, from free settling regime (SSC=0.02 g/L, no interactions between particles during their settling) to hindered regime (SSC=99.0 g/L, strong interactions between particles which hinder their settling). A complete description of all measurements is reported in the appendix (table A1).

| Sample n° | Type of conditions, step in parenthesis | Measured parameter | Instrument | Mean SSC (g · $L^{-1}$) (±5%) |
|---|---|---|---|---|
| 1a | Turbulent (1) | *Df* | LISST | 96.5 constant |
| 1b | Quiescent (2a) | $w_{s,q}$ | SCAF | 96.5 toward 0 |
| 1c | Settling (2b) | $w_{s,\neq}$ | SCAF | 96.5 toward 0 |
| 2a | Turbulent (1) | *Df* | LISST | 28.6 constant |
| 2b | Quiescent (2a) | $w_{s,q}$ | SCAF | 28.6 toward 0 |
| 2c | Settling (2b) | $w_{s,\neq}$ | SCAF | 28.6 toward 0 |
| 3a | Turbulent (1) | *Df* | LISST | 24.1 constant |
| 3b | Quiescent (2a) | $w_{s,q}$ | SCAF | 24.1 toward 0 |

| | | | | | |
|---|---|---|---|---|---|
| 3c | Settling | (2b) | $w_{s,\neq}$ | SCAF | 24.1 toward 0 |
| 4a | Turbulent | (1) | *Df* | LISST | 22.3 constant |
| 4b | Quiescent | (2a) | $w_{s,q}$ | SCAF | 22.3 toward 0 |
| 4c | Settling | (2b) | $w_{s,\neq}$ | SCAF | 22.3 toward 0 |
| 5a | Turbulent | (1) | *Df* | LISST | 18.1 constant |
| 5b | Quiescent | (2a) | $w_{s,q}$ | SCAF | 18.1 toward 0 |
| 5c | Settling | (2b) | $w_{s,\neq}$ | SCAF | 18.1 toward 0 |
| 6a | Turbulent | (1) | *Df* | LISST | 15.4 constant |
| 6b | Quiescent | (2a) | $w_{s,q}$ | SCAF | 15.4 toward 0 |
| 6c | Settling | (2b) | $w_{s,\neq}$ | SCAF | 15.4 toward 0 |
| 7a | Turbulent | (1) | *Df* | LISST | 13.4 constant |
| 7b | Quiescent | (2a) | $w_{s,q}$ | SCAF | 13.4 toward 0 |
| 7c | Settling | (2b) | $w_{s,\neq}$ | SCAF | 13.4 toward 0 |
| 8a | Turbulent | (1) | *Df* | LISST | 8.9 constant |
| 8b | Quiescent | (2a) | $w_{s,q}$ | SCAF | 8.9 toward 0 |
| 8c | Settling | (2b) | $w_{s,\neq}$ | SCAF | 8.9 toward 0 |
| 9a | Turbulent | (1) | *Df* | LISST | 6.9 constant |
| 9b | Quiescent | (2a) | $w_{s,q}$ | SCAF | 6.9 toward 0 |
| 9c | Settling | (2b) | $w_{s,\neq}$ | SCAF | 6.9 toward 0 |
| 10a | Turbulent | (1) | *Df* | LISST | 6.2 constant |
| 10b | Quiescent | (2a) | $w_{s,q}$ | SCAF | 6.2 toward 0 |
| 10c | Settling | (2b) | $w_{s,\neq}$ | SCAF | 6.2 toward 0 |
| 11a | Turbulent | (1) | *Df* | LISST | 6.2 constant |
| 11b | Quiescent | (2a) | $w_{s,q}$ | SCAF | 6.2 toward 0 |
| 11c | Settling | (2b) | $w_{s,\neq}$ | SCAF | 6.2 toward 0 |
| 12a | Turbulent | (1) | *Df* | LISST | 4.3 constant |
| 12b | Quiescent | (2a) | $w_{s,q}$ | SCAF | 4.3 toward 0 |
| 12c | Settling | (2b) | $w_{s,\neq}$ | SCAF | 4.3 toward 0 |
| 13a | Turbulent | (1) | *Df* | LISST | 4.3 constant |
| 13b | Quiescent | (2a) | $w_{s,q}$ | SCAF | 4.3 toward 0 |
| 13c | Settling | (2b) | $w_{s,\neq}$ | SCAF | 4.3 toward 0 |
| 14a | Turbulent | (1) | *Df* | LISST | 3.8 constant |
| 14b | Quiescent | (2a) | $w_{s,q}$ | SCAF | 3.8 toward 0 |
| 14c | Settling | (2b) | $w_{s,\neq}$ | SCAF | 3.8 toward 0 |
| 15a | Turbulent | (1) | *Df* | LISST | 2.7 constant |
| 15b | Quiescent | (2a) | $w_{s,q}$ | SCAF | 2.7 toward 0 |
| 15c | Settling | (2b) | $w_{s,\neq}$ | SCAF | 2.7 toward 0 |
| 16a | Turbulent | (1) | *Df* | LISST | 2.0 constant |
| 16b | Quiescent | (2a) | $w_{s,q}$ | SCAF | 2.0 toward 0 |
| 16c | Settling | (2b) | $w_{s,\neq}$ | SCAF | 2.0 toward 0 |
| 17a | Turbulent | (1) | *Df* | LISST | 2.0 constant |
| 17b | Quiescent | (2a) | $w_{s,q}$ | SCAF | 2.0 toward 0 |
| 17c | Settling | (2b) | $w_{s,\neq}$ | SCAF | 2.0 toward 0 |
| 18a | Turbulent | (1) | *Df* | LISST | 1.1 constant |
| 18b | Quiescent | (2a) | $w_{s,q}$ | SCAF | 1.1 toward 0 |
| 18c | Settling | (2b) | $w_{s,\neq}$ | SCAF | 1.1 toward 0 |
| 19a | Turbulent | (1) | *Df* | LISST | 0.89 constant |
| 19b | Quiescent | (2a) | $w_{s,q}$ | SCAF | 0.89 toward 0 |
| 19c | Settling | (2b) | $w_{s,\neq}$ | SCAF | 0.89 toward 0 |
| 20a | Turbulent | (1) | *Df* | LISST | 0.21 constant |

| | | | | | |
|---|---|---|---|---|---|
| 20b | Quiescent | (2a) | $ws_{surf}$ | SCAF | 0.21 toward 0 |
| 20c | Settling | (2b) | $ws_b$ $w_{s,\neq}$ | SCAF | 0.21 toward 0 |
| 21a | Turbulent | (1) | *Df* | LISST | 0.019 constant |
| 21b | Quiescent | (2a) | $w_{s,q}$ | SCAF | 0.019 decreasing |
| 21c | Settling | (2b) | $w_{s,\neq}$ | SCAF | 0.019 decreasing |

**Table A2.** Description of the physical conditions of the experiments conducted in the laboratory. For all runs, salinity was equal to 17. $w_{s,q}$ and $w_{s,\neq}$ correspond to settling velocity under "quiescent" and "settling" dominated conditions. The reader can refer to Wendling et al. (2015) for further details.

**Step 1: PSD under turbulent condtions.**

For each run, a volume of 2 litres of water sediment mixture was introduced into the rectangular base mixing jar tank (11.5 x 11.5 x 15 cm) and mixed with an impeller for thirty minutes. Experimental conditions promoting flocculation were obtained with the rotation of the impeller at 100 rpm, which corresponded to a mean turbulent energy dissipation parameter G of 44 $s^{-1}$.

A few mL of water sediment mixtures was then gently extracted from the mixing tank and put into sampling chamber housing the LISST XR portable instrument (Sequoia©) to measure the Particle Size Distribution (PSD). The time gap between sampling and measurements was of nearly 5 seconds.

**Step 2: settling velocity under quiescent conditions and flocculation by differential settlign.**

After measurements were taken under turbulent conditions, 160 mL of fluid-sediment mixture was pumped from the jar tank and placed in the SCAF settling tube to characterize flocculation under quiescent and settling conditions.

Measurements taken in the upper part of the SCAF settling tube during the first minutes provided an estimation of flocs settling velocity under quiescent conditions ws,q (**step 2a**), while measures realized near the bottom of the settling tube after several tens of minutes provided an estimation of flocs settling velocity by differential settling under settling dominated conditions ws,≠ (**step 2b**). The estimation of ws,q and ws,≠ was deduced following the methodology developed by Wendling et al. (2015) (Table A2). It is based on the local slopes of iso-turbidity lines near settling tube surface (ws,q) and near settling tube bottom (ws,≠).

## 2. Results (additional information to main text)

### 2.1. Influence of SSC on floc dynamics under turbulent dominated conditions

Typical PSDs measured in the experiments under turbulent conditions for low (SSC~20 mg/L), high (SSC~800 mg/L) and very high (SSC~2,000 mg/L) concentrations are shown in Figure A4 and illustrate the impact of increasing concentration on flocculation: at low concentration, the PSD exhibits a unimodal distribution (on a logarithmic scale) with a population of particles between 1.0 to 100 µm

and a median of 9.6 (±1) µm. In contrast to this, the method of Launay (2014) identified a bimodal distribution of the PSDs at high concentration (on a logarithmic scale). The finest population displays a similar distribution to that observed at low concentration with particles between 1 to 100 µm and a median of 12 (±2) µm. A second population develops for particles coarser than 100 µm. This second population has a median of 211 (±30) µm. The population of small particles predominates and corresponds to 90% of the total volume of particles (Fig. A4b). At very high concentration, the PSD obtained is broadly similar to that obtained at high concentration (Fig. A4c). The fine population has a median of 10.1 µm, while the median of the second population is 151 (±25) µm. As for the high concentration, the volumetric concentration of the small population also dominates (84% of the total volume).

Figures A4e and A4f show the PSD of the same samples after two minutes of sonication. The time gap between the end of sonication and measurements is about 5 seconds. The sonication broke the flocs, revealing the PSD of the elementary particles. In both cases, the larger particles disappeared, indicating the breakup of the large flocs. By replacing the original large flocs, three populations of particles are identified: one that was in the range of the first population before sonication, one smaller, and one slightly larger than this central population. Similar results were obtained for all laboratory samples with high SSC.

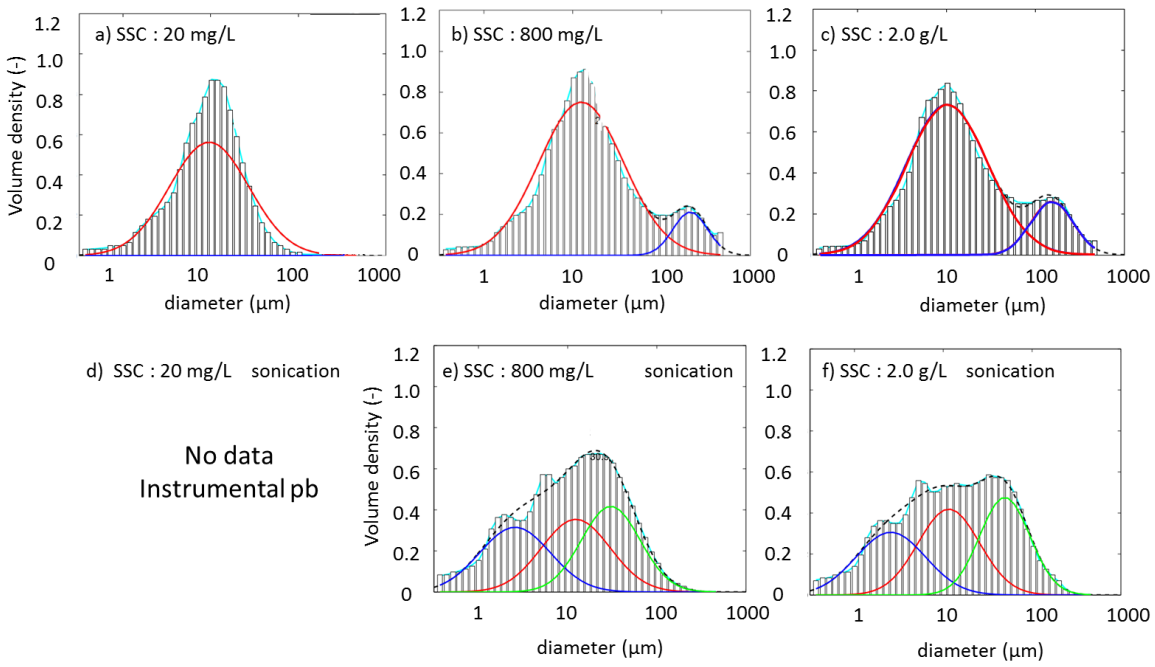


Fig. A4. Particle Size Distributions (PSD) of particles sampled during the jar tank experiment for low, high and very high SSC. These PSDs were obtained before sonication (4a, 4b, 4c) and after sonication (3e, 3f). Due to instrumental limitation, no data was acquired after sonication with LISST system for very low SSC (at 20 mg/L). Red, blue and green curves correspond to the identified sub-populations.

## 2.2. Influence of SSC on floc dynamics under quiescent and settling dominated conditions

Sedimentation, in SCAF settling column, for low (SSC ~ 20 mg $L^{-1}$), high (SSC ~ 800 mg $L^{-1}$) and very high (SSC ~ 2,000 mg $L^{-1}$) concentrations is reported in Figure A5. These graphs show the decrease of turbidity in the settling column over time and space. Complete sedimentation required about four hours for the run performed at low concentration (Fig. A5a) and less than one hour for runs conducted at high and very high concentrations (Fig. A5b and A5c).

In Figure A5, $w_{s,q}$ is about 1.1 $10^{-5}$ m/s for a SSC value of ~ 19 mg/L . It increases by an order of magnitude to 1.0 $10^{-4}$ m/s for high concentrations (SSC ~ 800 mg· $L^{-1}$), and shows an additional 40% increase for very high concentrations (SSC ~ 2000 mg/L for which $w_{s,q}$=1.4 $10^{-4}$ m $s^{-1}$). The settling velocity $w_{s,\neq}$ measured near bottom reaches values of 4.0 $10^{-5}$ m $s^{-1}$, 2.5 $10^{-4}$ m $s^{-1}$ and 1.0 $10^{-3}$ m $s^{-1}$, for the same SSC values of ~19, ~800 and ~2000 mg/L (i.e. a respective 3.6, 2.5 and 7.1 fold increase of the settling velocity caused by the flocculation by differential settling). As a preliminary conclusion, results presented in Figure A5 show that with increasing SSC, the settling velocity also increased as a result of flocculation.

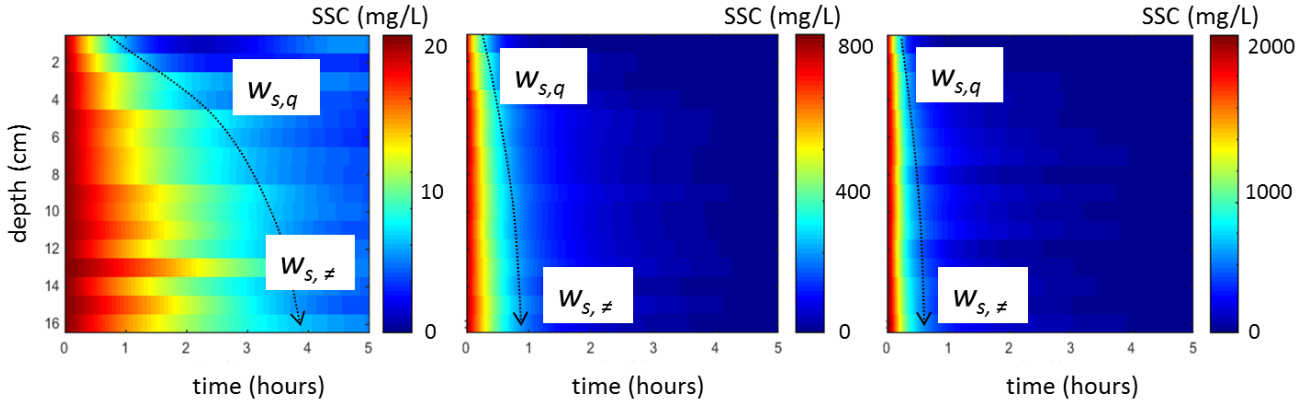


Fig. A5. Variation of SSC with time during the settling of particles measured by the SCAF instrument for low, high and very high SSC conditions.

Figure A6 compiles results from all experiments conducted under quiescent (ws,q) and settling (ws, ≠) conditions. The experimental curves of ws,q (SSC) and ws, ≠ (SSC) are well described by a semi empirical law of the form (Hwang and Mehta, 1989):

$$w_s = \begin{cases} w_{s\,free} & \text{SSC} < C_1 \\ a\,\dfrac{\text{SSC}^{\,n}}{(\text{SSC}^2+b^2)^m} & C_1 < \text{SSC} < C_{gel} \end{cases} \qquad (1)$$

where

$w_{s\,free}$ (m/s): free settling velocity

$a$: velocity scale coefficient

$n$: flocculation settling exponent

$b$: hindered settling coefficient

$m$: hindered settling exponent and

$C_1$ , $C_{gel}$ : zone concentration limits between free regime and flocculation regime, and hindered regime and consolidation regime, respectively.

The parameterization of $a, n, b, m,$ and $C_1$ was done by trial and error; fitting parameters are reported in Table A3. In our case, the gelling concentration (i.e. concentration beyond which a loose soil structure develops) was not reached (beyond 99.0 g/L). It typically appears when particles are deposited in the bed and start compacting.

| Settling conditions | $w_{s\,free}$ (m/s) | $a$ [-] | $n$ [-] | $b$ (g/L) | $m$ [-] | $C_1$ (g/L) | $C_{gel}$ (g/L) |
|---|---|---|---|---|---|---|---|
| $w_{s,q}$ | 1.3 $10^{-5}$ | 0.0045 | 1.25 | 6 | 1.05 | 0.2 | ? |
| $w_{s,\neq}$ | 3.5 $10^{-5}$ | 0.0025 | 1.7 | 2 | 1.2 | 0.2 | ? |

**Table. A3.** Fitted parameters for the application of Eq. 1

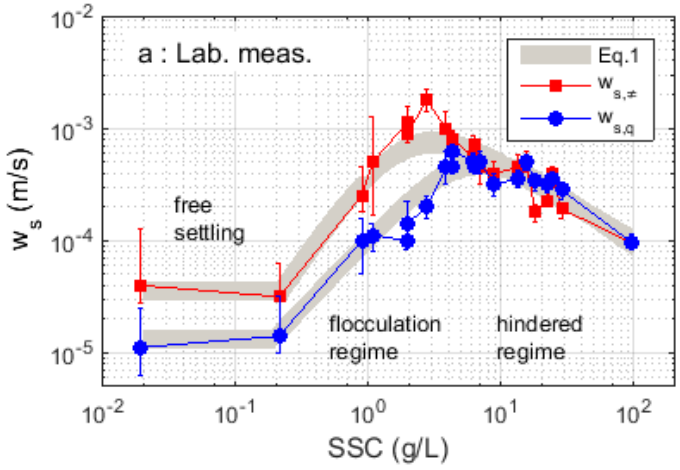


Fig. A6) Variation of the settling velocity of particles with suspended sediment concentration for a) laboratory conditions. Squares and circles correspond to settling velocity under quiescent and settling conditions, respectively. Grey lines correspond to interpolated settling laws according to Hwang and Mehta (1989).

## 2.3. Intercomparision of sediment fluxes with other estuarine and coastal zones in the world

In the main paper, we discuss the relative behavior of sediments from the Mekong delta, in comparison with other systems in the world. Table A4 provides the list of estuarine and coastal systems reported in the literature, that we used for this intercomparison.

| Site number and author(s) | Location and years of sampling | Country | Instrument |
|---|---|---|---|
| 1/2 Puls et al. (1988) | River Elbe 1985–1986 | Germany | Braystoke tube |
| 3/4 Puls et al. (1988) | River Weser 1985 | Germany | Braystoke tube |
| | River Tamar | | |
| 5/6/7 Barton et al. (1991) | 1986-1987-1988 | United Kingdom | Owen tube |
| 8/9/10 Edelvang and Larsen (1995) | Ho Bay 1989-1990 | Danish Wadden Sea | Braystoke tube |
| 11 Andersen (1999) | Rømø Bay 1997 | Danish Wadden Sea | Braystoke tube |
| 12 Burt (1986) | River Thames 1969–1983 | England | Owen tube |
| 13 Pejrup (1988) | Ho Bay and Rømø Bay 1983–1984 | Danish Wadden Sea | Braystoke tube |
| 14 Jones and Jago (1996) | River Elbe 1993 | Germany | QUISSET tube |
| 15 Pejrup and Edelvang (1996) | | | Braystoke tube |
| 16/17/18 Dyer et al. (1996) | River Elbe 1993 | Germany | Owen tube |
| 19 Thorn (1981) | Severn Estuary | UK | |
| 20 Ross (1988) | Tampa bay | USA | Settling column, by SSC sampling |
| 21 Sottolichio et al., (2011) | Gironde estuary 2007 | France | Bergen Nautik Sedimeter |
| 22 Gratiot and Anthony (2016) | Kaw river mouth, 2001 | French Guiana | Settling column, Bergen Nautik Sedimeter |
| 23 present study | Song Hau river mouth, 2015-2016 | Vietnam | SCAF settling tube |

**Table A4.** Sites and references for flocculation and settling velocity comparisons.

## Reference


Andersen, T.J., 1999. Suspended sediment transport and sediment reworking at an intertidal mudflat, the DanishWadden Sea. Meddelelser fra Skalling-Laboratoriet 37 Institute of Geography, University of Copenhagen.

Anthony, E. J., Brunier, G., Besset, M., Goichot, M., Dussouillez, P. and Nguyen V.L. 2015. Linking rapid erosion of the Mekong River delta to human activities. *Sci. Rep.* 5, 14745; (2015).

Barton, M.L., Stephens, J.A., Uncles, R.J., West, J.R., 1991. In: Elliott, M., Ducrotoy, J.P. (Eds.), Particle fall velocities and related variables in the Tamar Estuary. Estuaries and Coasts: Spatial and Temporal Intercomparisons. Olsen & Olsen, 31–36.

Bravard, J.P., Goichot, M. and Gaillot, S. 2013. Geography of sand and gravel mining in the Lower Mekong River. First survey and impact assessment. Echogéo, 26, 2–18.

Brunier, G., Anthony, E. J., Goichot, M., Provansal, M. & Dussouillez, P. 2014. Recent morphological changes in the Mekong and Bassac river channels, Mekong Delta: The marked impact of river-bed mining and implications for delta destabilisation. Geomorphology, 224, 177–191.

Burt, T.N., 1986. Field settling velocities of estuary muds. In: Mehta, A.J. (Ed.), Estuarine Cohesive Sediment Dynamics. Lecture Notes on Coastal and Estuarine Studies vol. 14. Springer-Verlag, 126–150.

Curran, K.J., Hill, P.S. and Milligan, T.G. 2003. Time variation of floc properties in a settling column. J. of Sea Res. 49, 1-9.

Darby, S.E., Hackney, C.R., Leyland, J., Kummu, M., Lauri, H., Parsons, D.R., Best, J.L., Nicholas, A.P. and Aalto, R. 2016. Fluvial sediment supply to a mega-delta reduced by shifting tropical-cyclone activity. Nature, 539(7628), 276.

Dyer, K.R., 1989. Sediment processes in estuaries: future research requirements. J. Geophys. Res. – Oceans. 94 C10 , 14327–14339.

Dyer, K.R., Cornelisse, J., Dearnaley, M.P., Fennessy, M.J., Jones, S.E., Kappenberg, J., McCave, I.N., Pejrup, M., Puls, W., van Leussen, W., Wolfstein, K., 1996. A comparison of in situ techniques for estuarine floc settling velocity measurements. J. Sea Res. 36, 15–29.

Edelvang, K., Larsen, M., 1995. The flocculation of fine-grained sediment in Ho Bugt, the Danish Wadden Sea. Folia Geographica Danica. Reitzels Forlag (TOM XXII.C.A.).

Gratiot, N., Coulaud, C., Legout, C., Mercier, B., Mora, H., Wendling, V., 2015. Unit for measuring the falling speed of particles in suspension in a fluid and device comprising at least one measuring unit and one automatic sampler. Patent-Publication number WO2015055963 A1

Gratiot, N. and Anthony, E.J. 2016. Role of flocculation and settling processes in development of the mangrove-colonized, Amazon-influenced mud-bank coast of South America. Mar. Geol., 373, 1-10.

Gratiot, N.; Michallet, H.; Mory, M. 2005. On the determination of the settling flux of cohesive sediments in a turbulent fluid. J. Geophys. Res. - Oceans. 110, No. C6, C06004.

Gratiot, N. and Manning, A.J 2004. An experimental investigation of floc's characteristics in a diffusive turbulent flow. Journal of Coastal Research, SI(41), 105-113.

Hill, P. S., Syvitski, J. P., Cowan, E. A., and Powell, R. D. 1998. In situ observations of floc settling velocities. Marine Geology, 145:85–94.

Hung, N. N., Delgado, J. M., Tri, V. K., Hung, L. M., Merz, B., Bárdossy, A. & Apel, H. 2012. Floodplain hydrology of the Mekong Delta, Vietnam. *Hydrological Processes,* 26**,** 674-686.

Hwang, K.-N. and Mehta, A. J. (1989). Fine sediment erodibility in Lake Okeechobee, Florida. Report ufl/coel-89/019, Department of Coastal and Oceanographic Engineering, University of Florida.

Jones, S.E., Jago, C.F., 1996. Determination of settling velocity in the Elbe estuary using QUISSET tubes. J. Sea Res. 36, 63-67.

Keyvani, A., Strom, K. 2014. Influence of cycles of high and low turbulent shear on the growth rate and equilibrium size of mud flocs. Marine Geol. 354, 1-14.

Koca K., Noss C., Anlanger C., Brand A., Lorke A., 2017. Peformance of the Vectrino Profiler at the sediment–water interface. Journal of Hydraulic Res. 55(4), 573-581.

Wendling, V., Gratiot, N., Legout, C., Droppo, I.G., Coulaud, C., Mercier, B. 2015. Using an optical settling column to assess suspension characteristics within the free, flocculation and hindered settling regimes. J. Soils and Sediment, (15) 1991-2003.

Kranenburg, C. 1994. The fractal structure of cohesive sediment aggregates, Estuar Coast Shelf S, 39, 451 – 460.

Kondolf, G.M., Rubin, Z.K. and Minear, J.T. 2014. Dams on the Mekong: cumulative sediment starvation. Water resource research, 50, 5158-5169.

Kumar, R. G., Strom, K. B., and Keyvani, A. 2010: Floc properties and settling velocity of San Jacinto estuary mud under variable shear and salinity conditions, Continental Shelf Res, 30, 2067-2081.

Launay, M. 2014. Flux de matières en suspension, de mercure et de PCB particulaires dans le Rhône, du Léman à la Méditerranée. Phd thesis. 434pp.

Lee, B.J., Toorman, E. and Fettweis, M. 2014. Multimodal particle size distributions of fine-grained sediments: mathematical modeling and field investigation. Ocean Dynamics. 64, 429-441.

Lick, W., Huang H. and Jepsen R. 1993. Flocculation of fine-grained sediments due to differential settling. J. Geophys. Res. - Oceans. 98, C6, 10,279-10,288.

Logan, B.E., 2012. Environmental transport processes. Wiley and Sons, 2nd edition, 464p.

Loisel H., A. Mangin, V.Vantrepotte, D.Dessailly, D.N.Dat, P.Gaernesson, S.Ouillon, J-P. Lefebvre, X.Mériaux, P.M. Thu. 2014. Analysis of the SPM concentration variability of the coastal waters under the Mekong's influence. Rem. Sens. of Envt 150, 218-230.

Manh, N.V., Dung, N.V., Hung, N.N., Merz, B., Apel, H. 2014. Large-scale suspended sediment transport and sediment deposition in the Mekong elta. HESS, 18, 3033-3053.

Manh, et al. 2015. Future sediment dynamics in the Mekong delta floodplains : Impacts of hydropower development, climate change and sea level rise. Global and Planetary Change. 127, 22-33.

Manning, A.J. and Dyer, K.R. 1999. A laboratory examination of floc characteristics with regard to turbulent shearing. Mar. Geol., 160, 146-170.

Mari, X., Torréton, J.P., Bich-Thuy Trinh, C., Bouvier, T., Thuoc, C.V., Lefebvre, J.-P., Ouillon, S., 2012. Aggregation dynamics along a salinity gradient in the Bach Dang estuary, North Vietnam. Estuar. Coast. Shelf Sci. 96, 151–158.

Mekong River Comm., 1 (Main Report), p. 254 (2011). Basin Development Plan Programme, Phase 2: Assessment of Basin-wide Development Scenarios. www.mrcmekong.org/assets/Publications/basin-reports/BDP-Assessment-of-Basin-wide-Dev-Scenarios-2011.pdf. (Accessed: 2 Mai 2017).

Mehta, A.H., 1989. On estuarine cohesive sediment suspension behavior. J. Geophys. Res. - Oceans, 94, C10, 14303-14314.

Mercier, B., Wendling, V., Coulaud, C., Legout, C., Gratiot, N., 2016. Développement d'un Système de Caractérisation des Agrégats et des Flocs (SCAF). c2i-2016 : 7ème Colloque Interdisciplinaire en Instrumentation. 20 21 Janvier 2016, Saint Nazaire, France, 8p.

Nowacki, D.J., Ogston, A.S., Nittrouer, C.A., Fricke, A.T. and Tri, V.P.D. 2015. Sediment dynamics in the lower Mekong river: transition from tidal river to estuary, J. Geophys. Res. - Oceans, 120, 6363-6383.

Pejrup, M., Mikkelsen, O.E., 2010. Factors controlling the field settling velocity of cohesive sediment in estuaries. Estuar. Coast. Shelf Sci. 87, 177–185.

Peteuil, C., Frétaud, T., Wirz, C., Camenen, B., Guertault, L., Le Coz, J., & Dramais, G. (2014). Importance of field observation for managing sediment fluxes in hydropower projects design and operation. In *Proceedings of the 19th IAHR-APD Congress, Hanoi, Vietnam*, 8pp.

.Puls, W., Kuehl, H., Heymann, K., 1988. Settling velocity of mud flocs: results of field measurements in the Elbe and the Weser Estuary. In: Dronkers, J., van Leussen, W. (Eds.), Physical Processes in Estuaries. Springer-Verlag, pp. 404–424.

Ross, M.A., 1988. Vertical structure of estuarine fine sediment suspensions. Technical Report. Coastal and Oceanographic Engineering Department, University of Florida, Gainesville.

Sottolichio, A., Hurther, D., Gratiot, N., Bretel, P., 2011. Acoustic turbulence measurements of near-bed suspended sediment dynamics in highly turbid waters of a macrotidal estuary. Continental Shelf Research, 31, S36-S49.

Thorn, M.F.C., 1981. Physical processes of siltation in tidal channels. Proceedings, Hydraulic Modelling Applied to Maritime Engineering Problems, ICE, London, UK, 47–55.

Tran, D. and Strom, K., 2017. Suspended clays and silts: are they independent or dependent fractions when it comes to settling in a turbulent suspension? Continental Shelf Research, 138, 81-94.

Valentin, C., Agus, F., Alamban, R., Bricquet, J.P, Chaplot, V., de Guzman, T., de Rouw, A., Janeau, J.L., Orange, D., Phachomphonh, K., Duy Phai, D., Podwojewski, P., Ribolzi, O., Silvaera, N., Subagyono, K., Thiébaux, J.P., Toan, T.D., and Vadari, T., 2008. Runoff and sediment losses from 27 upland catchments in Southeast Asia: Impact of rapid land use changes and conservation practices. Agriculture, ecosystems and environment. 128, 4, 225-238.

Verney, R., Lafite, R. and Brun-Cottan, J.C. 2009. Flocculation potential of estuarine particles: the importance of environmental factors and of the spatial and seasonal variability of suspended particulate matter. Estuaries and Coasts, 32, 678-693.

Wendling, V., Gratiot, N., Legout, C., Droppo, I.G., Coulaud, C. and Mercier, B. 2015. Using an optical settling column to assess suspension characteristics within the free, flocculation and hindered settling regimes. J. of Soils and Sediment, (15) 1991-2003.

Winterwerp, J.C. 2002. On the flocculation and settling of estuarine mud. Continental shelf research, 22, 1339-1360.

Wolanski, E., Ngoc Huan, N., Trong Dao, L., Huu Nhan, N. & Ngoc Thuy, N. 1996. Fine-sediment Dynamics in the Mekong River Estuary, Vietnam. Estuar. Coast. Shelf Sci., 43, 565-582.

Wolanski, E., Nhan, N.H. and Spagnol, S. 1998. Sediment dynamics during low flow conditions in the Mekong river estuary, Vietnam. Journal of Coastal Research, 14, 2, 472-482.